NANO LETTERS

pubs.acs.org/NanoLett

Ultrathin Spinel $LiMn_2O_4$ Nanowires as High Power Cathode Materials for Li-Ion Batteries

Hyun-Wook Lee,[†] P. Muralidharan,[†] Riccardo Ruffo,[‡] Claudio M. Mari,[‡] Yi Cui,[§] and Do Kyung Kim*[,†]

[†]Department of Materials Science and Engineering, Korea Advanced Institute of Science and Technology (KAIST), Daejeon 305-701, Korea, [‡]Dipartimento di Scienza dei Materiali, Università degli Studi di Milano-Bicocca, Milan 20125, Italy, and [§]Department of Materials Science and Engineering, Stanford University, Stanford, California 94305

ABSTRACT Ultrathin $LiMn_2O_4$ nanowires with cubic spinel structure were synthesized by using a solvothermal reaction to produce α-MnO_2 nanowire followed by solid-state lithiation. $LiMn_2O_4$ nanowires have diameters less than 10 nm and lengths of several micrometers. Galvanostatic battery testing showed that $LiMn_2O_4$ nanowires deliver 100 and 78 mAh/g at very high rate (60C and 150C, respectively) in a larger potential window with very good capacity retention and outstanding structural stability. Such performances are due to both the favorable morphology and the high crystallinity of nanowires.

KEYWORDS Energy storage, lithium ion battery, $LiMn_2O_4$ nanowires, high power density, Jahn−Teller distortion

The high energy and power density capability of lithium ion battery technology is attracting widespread interest over the past few years due to potential applications in both hybrid electric vehicles (HEV) and full electric vehicles (EV).[1−3] Although lithium ion batteries can provide higher energy density (W h/kg) than other secondary systems, they have limited power density (W/kg) compared to double layer and pseudocapacitors.[4] Hence the improvement of the specific power density in lithium ion batteries is a fundamental issue to develop better HEVs and EVs. Spinel $LiMn_2O_4$ is a promising candidate to replace layered Ni or Co oxide materials as cathode in lithium ion batteries because of its intrinsic low-cost, environmental friendliness, high abundance, and better safety.[5−9] However, the application of $LiMn_2O_4$ in high power systems requires the development of fast kinetic electrodes which appears nowadays possible thanks to the use of nanostructured morphologies.

Various approaches have been widely investigated to enhance the power density using nanostructured materials[10−14] or core shell structures coated with oxide or fluoride.[15,16] In our previous work,[17,18] we verified that the one-dimensional nanosized materials have faster kinetics and higher rate capability than micrometer-sized materials due to the large surface-to-volume ratio that enhances the contact between active material grains and electrolyte. In particular, $LiMn_2O_4$ nanorods with 150 nm diameter showed good capacity retention (around 60%) up to 5C.[18] Furthermore, a few nanometer sized systems operate differently in comparison to bulk materials in terms of electrical and chemical properties.[19] Indeed it has been demonstrated than nanosized spinel $LiMn_2O_4$ structures can transform between cubic and tetragonal phases with facile strain relaxation.[20,21] Consequently, we believe ultrathin nanowire $LiMn_2O_4$ is a promising cathode material for lithium ion batteries for HEV and EV applications thanks to its high rate capability and superior structural stability.

Generally, the electrochemical performances of electrode materials are strongly influenced by the phase crystallinity, purity, particle size, and distribution. These significant factors depend on preparation approaches.[3] A traditional solid state reaction method was used to produce high crystalline $LiMn_2O_4$, but it requires high temperature calcinations (about 800 °C) and long times, which cause a coarsening of the powders with a broad grain size distribution.[22] As a consequence, a number of soft chemistry techniques have been explored to prepare $LiMn_2O_4$, such as sol−gel,[23] solution phase,[24] and combustion.[25,26] Although uniform $LiMn_2O_4$ particles with good electrochemical performance could be thus obtained, the synthetic procedures are generally complex and costly. Therefore, to synthesize high power capable nanosized materials, it is highly recommended to develop a simple and scalable method like the solid state reaction route.

α-Manganese oxide (α-MnO_2) was reported to have a particular one-dimensional structure which can be synthesized as 5−10 nm diameter nanowires.[27] Hence, it has been considered as a possible precursor to produce $LiMn_2O_4$ nanosized electrode materials.[28,29] However, often the low crystallinity of α-MnO_2 affects the grain size distribution of the lithiated phase and maintaining the α-MnO_2 precursor nanowire morphology during phase transformation is a formidable challenge. Chemical lithiation of transition metal oxides has been reported to enhance the performance of a Li-ion battery without significant change of oxide morphology.[30,31]

* To whom correspondence should be addressed, dkkim@kaist.ac.kr.
Received for review: 03/25/2010
Published on Web: 08/26/2010

DOI: 10.1021/nl101047f | *Nano Lett.* **2010,** *10,* 3852–3856

In this paper, we successfully synthesized ultrathin spinel $LiMn_2O_4$ nanowires using a facile, easy to scale up two-step process: a solvothermal reaction to prepare α-MnO_2 nanowires followed by solid state reaction with LiOH. The nanowire structure and morphology have been correlated to the electrochemical characterization and the possibility of high rate capability as well as phase stability was demonstrated.

The synthesis of ultrathin $LiMn_2O_4$ nanowires was carried out by a two-step approach. First α-MnO_2 nanowires were prepared starting from acetate precursor by solvothermal reaction without the use of catalysts and templates. In the successive step $LiMn_2O_4$ phase was obtained by solid state reaction between the prepared α-MnO_2 nanowires and LiOH at low pressure in oxygen atmosphere. The structures and morphologies of α-MnO_2 and $LiMn_2O_4$ nanowires were characterized by X-ray diffraction (XRD), scanning electron microscopy (FE-SEM), and high resolution transmission electron microscopy (HR-TEM). For the electrochemical investigation, electrodes were obtained with 75 wt % $LiMn_2O_4$ active material nanowires, 17 wt % conductive carbon black, and 8 wt % organic binder, and they were tested in half cell vs lithium using 2032 type coin cells. In the following all the potential values will be reported against Li^+/Li couple. Details about materials preparation and experimental procedures are given in the Supporting Information.

The synchrotron XRD pattern of the prepared α-MnO_2 was indexed to a pure tetragonal phase (*I*4/*m*, space group 87) which corresponds to JCPDS data No. 44-0141 (Figure 1a). The morphology of α-MnO_2 nanowires is confirmed by the FE-SEM and FE-TEM images (Figure 1b,c). As one can observe, well-dispersed nanowires have homogeneous diameter sizes (8−9 nm) and lengths of several micrometers. The HR-TEM image of a single nanowire (Figure 1d) indicates that the nanowire is structurally uniform and highly crystalline; the lattice spacing of 0.69 nm is consistent with that of the α-MnO_2 (110) plane. The surface area of the α-MnO_2 nanowires estimated by the BET method was 110.9 m^2/g with a correlation coefficient of 0.9999.

Ultrathin $LiMn_2O_4$ nanowires were obtained by solid state reaction under low pressure from α-MnO_2 nanowires using solid state reaction. The high-resolution synchrotron XRD diffrattogram of $LiMn_2O_4$ nanowires (Figure 1e) shows the feature of the spinel structure with cubic phase (*Fd*$\bar{3}$*m*, space group 227, JCPDS data No. 35-0782). No peaks of the α-MnO_2 precursor phase and other impurities were detected even though the nanowires were synthesized at a relatively lower temperature than typical reaction temperature of spinel $LiMn_2O_4$.[28] Besides, the surface area of $LiMn_2O_4$ nanowires estimated by BET method was 95.6 m^2/g (correlation coefficient of 0.9937), which is comparable to that of α-MnO_2 nanowires. Panels f and g of Figure 1 show the SEM image and HR-TEM image of the synthesized $LiMn_2O_4$ nanowires. The high-quality cubic spinel $LiMn_2O_4$ nanowires were well-dispersed and maintained dimensions and morphology of α-MnO_2 nanowire precursor. In Figure 1h, fast Fourier transform (FFT) analysis was performed on the lattice fringe from the Figure 1g and the diffraction spots well match the [220] lattice direction of $LiMn_2O_4$ revealing single crystalline nanowires. This indicates that the solid state lithiation process is able to change the phase from the tetragonal structure of α-MnO_2 to the cubic structure of spinel $LiMn_2O_4$ without changing the nanowire morphology and size.

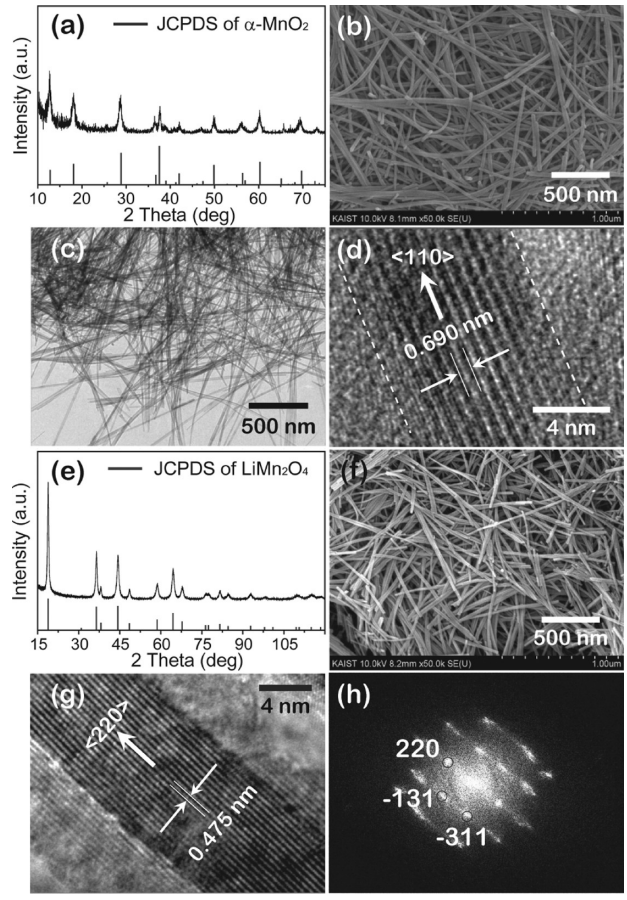

FIGURE 1. (a) XRD pattern, (b) SEM image, (c) TEM, and (d) HR-TEM images of α-MnO_2 as obtained from solvothermal reaction. (e) XRD pattern, (f) SEM image, (g) HR-TEM of $LiMn_2O_4$ as obtained from solid state reaction. (h) FFT analysis of the lattice fringes in (g).

Coin-type cell configuration was used to evaluate the electrochemical properties of the materials as cathode electrode. Representative charge−discharge curves of the spinel $LiMn_2O_4$ nanowires are shown in Figure 2a (fifth cycle). The cell was cycled at current density of 14.8 mA/g (0.1C rate) in the potential range 3.5/4.3 V. Both the charge and discharge curves exhibited two pseudoplateaus at around 3.9 and 4.1 V which represent the typical electrochemical behavior of spinel $LiMn_2O_4$.[17] The charge capacity is about 128 mAh/g, and the discharge capacity is about 125 mAh/g, showing a Coulombic efficiency of 98% (above 90% at the first cycle). To further investigate the application in high power density devices, the cell was discharged at different rates ranging from 1C (148 mA/g) to 30C (4440 mA/g), using

DOI: 10.1021/nl101047f | *Nano Lett.* **2010,** *10,* 3852--3856

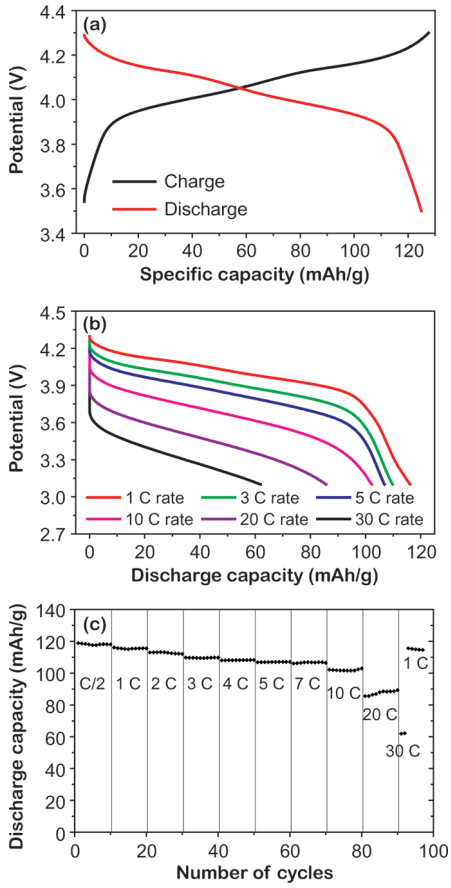

FIGURE 2. (a) Characteristic low rate (C/10) charge/discharge curves. (b) Discharge curves at different rates after charging at 1C. (c) Discharge capacity as function of cycle numbers of $LiMn_2O_4$ nanowire electrode cycled in the 3.1/4.3 V potential range.

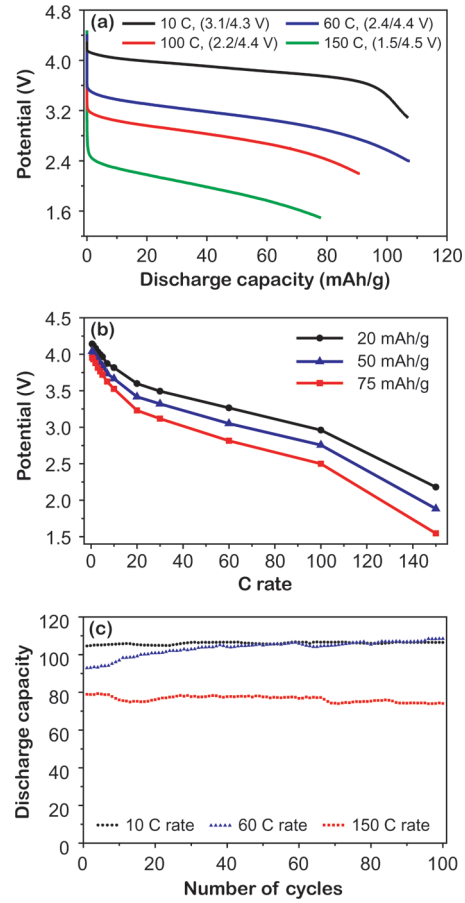

FIGURE 3. (a) Discharge curves at different rates after charging at 1C. (b) Potential vs C/rate at three different capacities. (c) Discharge capacity as function of cycle numbers of $LiMn_2O_4$ nanowire electrode cycled in different potential ranges.

a 1C charge rate (Figure 2b). Discharge capacity of the $LiMn_2O_4$ nanowire cathode decreases to 116, 110, 107, 102, 86, and 62 mAh/g when current rate increases to 1, 3, 5, 10, 20, and 30C, respectively (Figure 2c). Remarkably, the capacities at 10C (1.48 A/g) and 20C (2.96 A/g) are still 102 and 86 mAh/g, respectively; at 30C (4.44 A/g) it drops to 62 mAh/g but then, after this high rate measurement, the nanowire cell is able to supply again the previously measured value (115 mAh/g) at 1 C rate, as an indication of the high reversibility of the system. When the charge and discharge processes were carried out at the same rate, we still observed good specific capacities up to 10C with 99.9% Coulomb efficiency (see Figure S1 in the Supporting Information). The capacity retention is much higher compared to previously reported $LiMn_2O_4$ nanorods.[18]

As the current rate increases, the pseudoplateau of each discharge curve moved downward. In fact at low rates, the cell operates close to equilibrium conditions, whereas at high currents, electrode overpotentials and the internal *IR* drop, mainly due to the low conductive organic electrolyte, increase thus decreasing the operating voltage of the cell.[32] To fully evaluate the delivering capability of the nanowires despite the voltage drops, ultrathin $LiMn_2O_4$ nanowire based cells were evaluated upon cycling in different potential windows at various rates (Figure 3a). According to the increase of the discharge current rate to 60C (8.88 A/g), 100C (14.8A/g), and 150C (22.2 A/g), the discharge voltage windows were enlarged to 2.4/4.4 V, 2.2/4.4 V, and 1.5/4.5 V, respectively. Even at very high current rates such as 100 and 150C, the discharge curves show the characteristic features of $LiMn_2O_4$ discharge profiles with an almost flat potential plateau. Figure 3b shows the potential drops of the nanowire cell at three different discharge states corresponding to capacity values of 20, 50, and 75 mAh/g, respectively. The graphs of potential drops confirm that the overvoltage of the cell is larger than 1.0 V at very high current rates (above 60C). Three electrode measurements are in progress to separate the lithium counter electrode polarization contribution to the overall cell voltage drop. To evaluate the cycling behavior at this high rate, conditions up to 100 cycles were performed, using 1C charge rate. The discharge capacity of $LiMn_2O_4$ nanowires shows very good capacity retention as one can observe in Figure 3c. The average discharge capacity of the current rate of 10C is around 105 mAh/g and those of the 60C and 150C are around 100 and 78 mAh/g, respectively. By the way, in the case of the 60C rate, the

DOI: 10.1021/nl101047f | *Nano Lett.* **2010,** *10,* 3852–3856

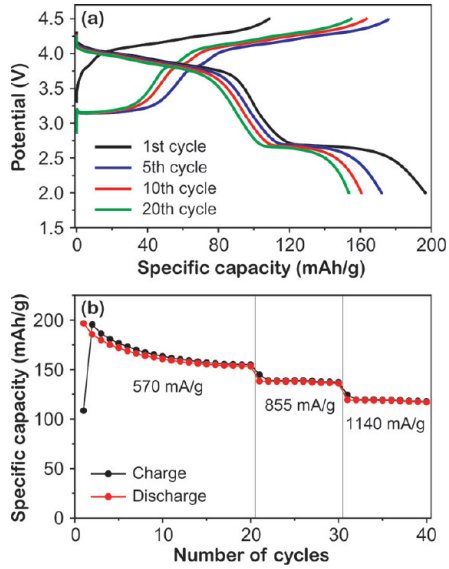

FIGURE 4. (a) Characteristic charge/discharge curves at 570 mA/g and (b) discharge capacity as function of cycle numbers at of $LiMn_2O_4$ nanowire electrode cycled in large compositional range.

discharge capacity gets an increase during the first 50 cycles. The result is probably to the counter electrode (Li metal) overpotential which decreases after several cycles (see Figure S2 in the Supporting Information). Therefore, the synthesized $LiMn_2O_4$ nanowires can be cycled at very high current rate in order to be used in high power applications.

To better understand the merits of ultrathin nanowire, it is useful to investigate the system also in larger compositional range. It is well-known that Li ions can be intercalated in the empty octahedral sites of the $LiMn_2O_4$ spinel structure to form $Li_{1+x}Mn_2O_4$. In titration experiments or at very low rate, a characteristic plateau around 3.0 V is observed.[33] Generally, the materials have a drastic capacity loss when the electrode is cycled in this compositional range.[34] In fact, the lowest potential plateau corresponds to the equilibrium between the cubic $LiMn_2O_4$ and the tetragonal $Li_2Mn_2O_4$ structure. $Li_2Mn_2O_4$ undergoes Jahn−Teller distortion which strongly affects the reversibility of the system. Moreover, when the single cubic phase changes to the tetragonal phase, *a* axis shrinks about 3% and *c* axis expands 12%,[33] which causes to severe loss of capacity, especially at a high rate. Figure 4a shows a charge and discharge curve of $LiMn_2O_4$ nanowires at a constant current of 570 mA/g. In addition to the high potential behavior (3.5/4.3 V), the curves show the low potential plateau (around 3 V), which corresponds to the structural change between cubic and tetragonal phase. Nevertheless, after 20 cycles, the capacity retention is 78% with an average Coulombic efficiency of 98%. The charge and discharge capacities vs number of cycles are reported in Figure 4b. The discharge capacities at a different current rates of 570, 855, and 1140 mA/g are 155, 137, and 118 mAh/g, respectively. Although the ultrathin $LiMn_2O_4$ nanowires undergo the harsh condition of the fast structural

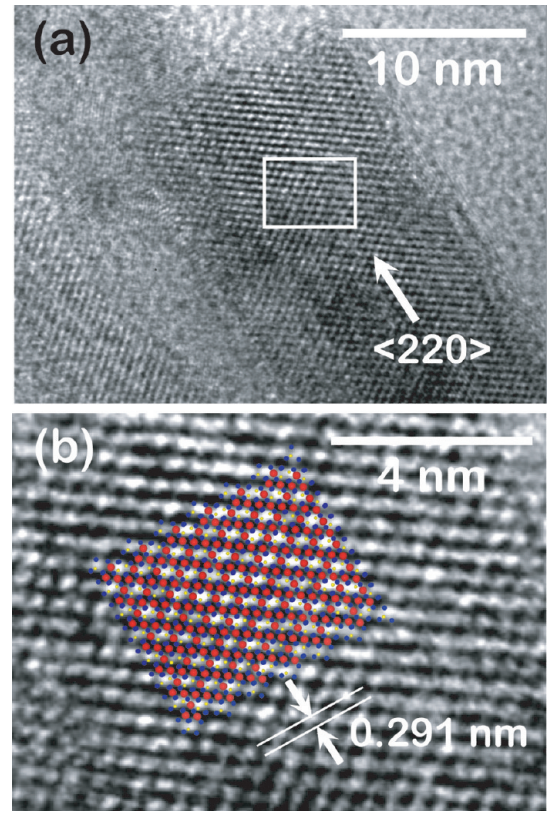

FIGURE 5. (a) High-resolution TEM images showing the cubic lattice structure of $LiMn_2O_4$ and (b) magnified image of (a) (white rectangular region) showing the match between the model and observed structure.

change from cubic to tetragonal structure and vice versa, the cell shows good capacity retention with high reversibility.

The very good performances of ultrathin $LiMn_2O_4$ nanowires at high current rate and in large compositional range can be understood in terms of morphological and structural features. $LiMn_2O_4$ has a three-dimensional lithium diffusion path due to favorable spinel cubic structure, so every plane is suitable to exchange lithium ion from active materials to the electrolyte. In addition, the nanowire has a large surface area and the merit of the one-dimensional electron transport. It is generally considered that low synthesis temperature leads to poor crystallinity product, which causes lower capacities.[35] The HR-TEM images in Figure 5a show that the $LiMn_2O_4$ nanowires have single crystalline habit and match with cubic structure. In Figure 5b, we highlight the lattice of $LiMn_2O_4$ structure using a cubic spinel model. When the model is tilted to ⟨110⟩ direction, the structure matches the HR-TEM image of $LiMn_2O_4$ lattice, which means that $LiMn_2O_4$ nanowires do not have any structural distortion. For the second issue (lattice expansion during phase equilibrium), the size of nanowire is considered. The distance from the surface to the inside is less than 5 nm, so the nanowire is able to shrink and expand lattice parameters in a more facile fashion than the bulk materials.[34] The very good performances in terms of fast kinetic and high reversibility

DOI: 10.1021/nl101047f | *Nano Lett.* **2010,** *10,* 3852–3856

on large compositional range are obtained thanks to a few nanometer-sized materials with high crystallinity.

Ultrathin spinel $LiMn_2O_4$ nanowires have been synthesized by solid state reaction under low pressure starting from α-MnO_2 nanowires. The complete structural change to spinel $LiMn_2O_4$ from the precursor has been observed by high-resolution synchrotron XRD, FE-SEM, and FE-TEM. The results have shown that thin-nanowire precursor morphology is preserved after the solid state reaction. As produced $LiMn_2O_4$ nanowires have around 10 nm diameter, and they are several micrometers in length. Such morphology improves the kinetic properties at very high current rate and was capable of the facile structural transformation of the cubic and tetragonal phase in the large compositional range. When charged at 1C the electrode shows a discharge specific capacity of about 90 mAh/g at 20C between 3.1 and 4.3 V vs Li. When the cycling potential range is enlarged to overcome electrode kinetic limitations, nanowires are able to deliver relevant discharge capacities (around 80 mAh/g) even at an extremely high current density (22.2 A/g, 150C rate), with high reversibility and good capacity retention.

Acknowledgment. This work was supported by the Center for Inorganic Photovoltaic Materials (No. 2008-0062206), Korea Science and Engineering Foundation (KOSEF) grant (No. R01-2008-000-20480-0), and "The Support Program for the Advancement of National Research Facilities and Equipment", funded by the Korean government (MEST). P.M. was financially supported by the Priority Research Centers Program through the National Research Foundation of Korea (NRF) funded by the Ministry of Education, Science and Technology (2009-0094041). The authors thank the Pohang Light Source, Korea for extending the synchrotron XRD for characterization.

Supporting Information Available. Details of ultrathin $LiMn_2O_4$ nanowire synthesis, sample preparation, and electrochemical supporting data. This material is available free of charge via the Internet at http://pubs.acs.org.

REFERENCES AND NOTES

(1) Tarascon, J. M.; Armand, M. *Nature* **2001**, *414* (6861), 359–367.
(2) Kang, K.; Meng, Y. S.; Berger, J.; Grey, C. P.; Ceder, G. *Science* **2006**, *311* (5763), 977–980.
(3) Whittingham, M. S. *Chem. Rev.* **2004**, *104* (10), 4271–4301.
(4) Whittingham, M. S. *MRS Bull.* **2008**, *33*, 411–419.
(5) Aricò, A. S.; Bruce, P.; Scrosati, B.; Tarascon, J. M.; Van Schalkwijk, T. *Nat. Mater.* **2005**, *5*, 366–377.
(6) Bruce, P.; Scrosati, B.; Tarascon, J. M. *Angew. Chem., Int. Ed.* **2008**, *47*, 2930–2946.
(7) Gummow, R. J.; Dekock, A.; Thackeray, M. M. *Solid State Ionics* **1994**, *69*, 59–67.
(8) Xia, Y. Y.; Yoshio, M. *J. Electrochem. Soc.* **1997**, *144*, 4186–4194.
(9) Amatucci, G.; Tarascon, J. M. *J. Electrochem. Soc.* **2002**, *149*, K31–K46.
(10) Shaju, K. M.; Jiao, F.; Debart, A.; Bruce, P. G. *Phys. Chem. Chem. Phys.* **2007**, *9*, 1837–1842.
(11) Li, N.; Patrissi, C. J.; Che, G.; Martin, C. R. *J. Electrochem. Soc.* **2000**, *147*, 2044–2049.
(12) Wang, Y.; Cao, G. Z. *Chem. Mater.* **2006**, *18*, 2787–2804.
(13) Li, Y.; Tan, B.; Wu, Y. *Nano Lett.* **2008**, *1*, 265–270.
(14) Lee, Y. J.; Kim, M. G.; Cho, J. *Nano Lett.* **2008**, *3*, 957–961.
(15) Cho, J. *J. Mater. Chem.* **2008**, *18* (19), 2257–2261.
(16) Kim, H. B.; Park, B. C.; Myung, S. T.; Amine, K.; Prakash, J.; Sun, Y. K. *J. Power Sources* **2008**, *179*, 347–350.
(17) Kim, D. K.; Muralidharan, P.; Lee, H. W.; Ruffo, R.; Yang, Y.; Chan, C. K.; Peng, H.; Huggins, R. A.; Cui, Y. *Nano Lett.* **2008**, *8* (11), 3948–3952.
(18) Yang, Y.; Xie, C.; Ruffo, R.; Peng, H.; Kim, D. K.; Cui, Y. *Nano Lett.* **2009**, *9* (12), 4109–4114.
(19) Lieber, C. M. *Solid State Commun.* **1998**, *107* (11), 607–616.
(20) Shao-Horn, Y.; Hackney, S. A.; Armstrong, A. R.; Bruce, P. G.; Gitzendanner, R.; Johnson, C. S.; Thackeray, M. M. *J. Electrochem. Soc.* **1999**, *146* (7), 2404–2412.
(21) Wang, H. F.; Jang, Y. I.; Chiang, Y. M. *Electrochem. Solid-State Lett.* **1999**, *2* (10), 490–493.
(22) Cabana, J.; Valdés-Solís, T.; Palacín, M. R.; Oró-Solé, J.; Fuertes, A.; Marbán, G.; Fuertes, A. B. *J. Power Sources* **2007**, *166* (2), 492–498.
(23) Curtis, C. J.; Wang, J. X.; Schulz, D. L. *J. Electrochem. Soc.* **2004**, *151* (4), 590–598.
(24) Nieto, S.; Majumder, S. B.; Katiyar, R. S. *J. Power Sources* **2004**, *136* (1), 88–98.
(25) Du, K.; Zhang, H. *J. Alloys Compd.* **2003**, *352* (1−2), 250–254.
(26) Kovacheva, D.; Gadjov, H.; Petrov, K.; Mandal, S.; Lazarraga, M. G.; Pascual, L.; Amarilla, J. M.; Rojas, R. M.; Herrero, P.; Rojo, J. M. *J. Mater. Chem.* **2002**, *12* (4), 1184–1188.
(27) Wang, X.; Li, Y. D. *J. Am. Chem. Soc.* **2002**, *124* (12), 2880–2881.
(28) Fang, H.; Li, L.; Yang, Y.; Yan, G.; Li, G. *J. Power Sources* **2008**, *184*, 494–497.
(29) Lim, S.; Cho, J. *Electrochem. Commun.* **2008**, *10*, 1478–1481.
(30) Garcia, B.; Millet, M.; Pereira-Ramos, J. P.; Baffier, N.; Bloch, D. *J. Power Sources* **1999**, *81−82*, 670–674.
(31) Mai, L.; Hu, B.; Chen, W.; Qi, Y.; Lao, C.; Yang, R.; Dai, Y.; Wang, Z. L. *Adv. Mater.* **2007**, *19*, 3712–3716.
(32) Linden, D.; Reddy, T. B. In *Handbook of Batteries*, 3rd ed.; McGraw-Hill: New York, 2002; pp 2.1−2.37.
(33) Ohzuku, T.; Kitagawa, M.; Hirai, T. *J. Electrochem. Soc.* **1990**, *137* (3), 769–775.
(34) Jiao, F.; Bao, J.; Hill, A. H.; Bruce, P. G. *Angew. Chem., Int. Ed.* **2008**, *47* (50), 9711–9716.
(35) Hosono, E.; Kudo, T.; Honma, I.; Matsuda, H.; Zhou, H. *Nano Lett.* **2009**, *9* (3), 1045–1051.

DOI: 10.1021/nl101047f | *Nano Lett.* **2010,** *10,* 3852–-3856